Carbohydrate Polymers 90 (2012) 392–398

Contents lists available at SciVerse ScienceDirect

Carbohydrate Polymers

journal homepage: www.elsevier.com/locate/carbpol

Inhibition on calcium oxalate crystallization and repair on injured renal epithelial cells of degraded soybean polysaccharide

Yao Xiu-Qiong[a], Ouyang Jian-Ming[a,*], Peng Hua[a], Zhu Wen-Yu[a], Chen He-Qun[b]

[a] Institute of Biomineralization and Lithiasis Research, Jinan University, Guangzhou 510632, China
[b] Department of Urology, Xiang Ya Hospital, Central Southern University, Changsha 410008, China

ARTICLE INFO

Article history:
Received 11 February 2012
Received in revised form 14 May 2012
Accepted 18 May 2012
Available online 5 June 2012

Keywords:
Soybean polysaccharide
Calcium oxalate
Cell repair
Biomineralization
ICP

ABSTRACT

This paper investigated the inhibitory effect of degraded soybean polysaccharide (DPS) on the growth of calcium oxalate (CaOxa) crystals. The results were compared with that of soybean polysaccharide without degradation (SPS). The data showed that DPS exhibited a much higher efficiency to inhibit CaOxa growth and stabilize calcium oxalate dihydrate (COD) compared with SPS. As DPS concentration increased, the soluble Ca^{2+} ions significantly increased, the aggregation degree of calcium oxalate monohydrate (COM) crystals decreased, the shape of COD crystals became round and blunt, and the Zeta potential on CaOxa crystal surface reduced. The above results were all conducive for the inhibition of CaOxa crystallization. In addition, DPS displayed a distinct repairing effect on oxidative injured renal epithelial cells in African green monkey (Vero), with enhanced cell viability and extracellular superoxide dismutase activity after repair. The morphologies of the repaired cells and their regulatory capability on CaOxa growth were between the control and injured cells. The results indicated that the risk of stone formation can be reduced by DPS, and that DPS may be a potential green drug to prevent the formation of CaOxa stones.

1. Introduction

Urinary stone is a frequently occurring clinical disease, and its main component is calcium oxalate (CaOxa) (Yasir & Waqar, 2011). Although drugs such as citric acid salt can be used for treatment, their therapeutic mechanisms have not yet been properly understood. Therefore, developing novel, highly effective, less toxic, and cheap anti-stone drugs is of great scientific and practical significance.

Soybean polysaccharides (SPS) are water-soluble polysaccharides that are extracted and refined from soybeans, and they belong to acid polysaccharides (Funami et al., 2008; Li, Matsumoto, Nakamura, Maeda, & Matsumura, 2009; Lu, Hou, & Ouyang, 2010). SPS contains an acid glycosyl main chain composed of galacturonic acids and a neutral glycosyl side chain containing arabinose. Its physicochemical properties and molecular structure are similar to those of glycosaminoglycans, which are the urolith inhibitors in urine. In addition, SPS can eliminate hydroxyl radicals, which makes SPS a potential green exogenous drug for the prevention and treatment of urolithiasis. Studies in vitro showed that SPS can inhibit the aggregation of calcium oxalate monohydrate (COM) crystals and induce the formation of calcium oxalate dihydrate (COD) crystals (Lu, Hou, & Ouyang, 2010).

However, natural SPS encounters difficulty in penetrating the cell membranes to exert its biological effects due to its high molecular weight and large molecular size (Le, Yin, & Xu, 2006), which results in its restricted clinical application. On the other hand, the biological activity of natural polysaccharides may be improved by degradation. For example, degraded sulfuric acid polysaccharide from spirulina, with low molecular weight, exhibits better antitumor activity than its un-degraded counterparts in vitro (Le, Yin, & Xu, 2006). Compared with ordinary heparin, heparin with low molecular weight exhibits a higher bioavailability and can inhibit atherosclerosis (Holmer, Kurachi, & Sodertrom, 2002). Degraded sulfuric acid polysaccharide from seaweed, with low molecular weight, exhibits a significantly higher ability to inhibit CaOxa formation than the un-degraded polysaccharide with high molecular weight (Ouyang, Wang, Lu, & Tan, 2010).

SPS was degraded with hydrogen peroxide in a previous study (Yao, Tan, Lu, & Ouyang, 2011). After degradation, the average molecular weight, carboxyl content, and intrinsic viscosity [η] of SPS decreased from 115,200, 13.8%, and 0.498 L/g to 10,200, 11.8%, and 0.1056 L/g, respectively, whereas the solubility of the degraded SPS increased from 8 g/L to 40 g/L.

Cell damage plays a major role in kidney stone formation (Lee et al., 2011; Yu et al., 2011). In previous papers (Ouyang, Yao, Tan, & Wang, 2011; Yao, Deng, & Ouyang, 2011; Zhang et al., 2012), two kinds of cell lines were used to study the effect of cell damage on the formation of CaOxa crystals, particularly HKC, which was an optimized and differentiated human renal proximal tubular

* Corresponding author.
E-mail address: toyjm@jnu.edu.cn (J.-M. Ouyang).

0144-8617/$ – see front matter © 2012 Elsevier Ltd. All rights reserved.
http://dx.doi.org/10.1016/j.carbpol.2012.05.056

epithelial cells, and Vero, which was obtained from the renal epithelial cells of an African green monkey. The results suggest that injured HKC induces stone formation by providing more nucleating sites for crystals, by promoting the aggregation of crystals, and by inducing the formation of COM crystals (Yao, Deng, et al., 2011; Zhang et al., 2012). The crystals induced by the injured Vero are the mixture of COD and COM crystals, which exhibit irregular shapes with sharp edges, whereas the crystals induced by the cells in the control group are mainly COD crystals with round edges and smooth surfaces (Ouyang et al., 2011). After incubation in CaOxa supersaturated solution for a considerable length of time, the Vero cells in the control group can also be subjected to injury, and then promote the growth of crystals, suggesting that the retention of high concentration of CaOxa in the urinary tract is a risk factor for the formation of kidney stones in vivo. Furthermore, the injured cells cause the formation of kidney stones because they promote the formation of harmful crystals and enhance the adhesion to crystals.

Exogenous polysaccharide molecules can repair damaged cells (Matsuo, 2008; Yao, Peng, Tan, & Ouyang, 2012) because they contain some negatively charged groups, such as —OH, $-SO_3H$, and —COOH (Ouyang et al., 2010), which can reduce the loss of the negative charge on the cell surface and repair the charge barrier, among others.

Based on the previous study, degraded polysaccharide (DPS) can inhibit the growth and aggregation of CaOxa crystals. The current study used DPS to repair the injured Vero cells, and compared the differences among the three states of Vero, namely, normal, injured, and repaired, in regulating CaOxa crystal growth, to discuss further the mechanism of kidney stone formation and then provide experimental evidence for the development of new anti-stone drugs.

2. Experiment

2.1. Reagents

SPS was extracted and refined from soybeans as previously described (Lu, Hou, & Ouyang, 2010), and DPS was obtained via the hydrogen peroxide degradation method. The basic parameters of SPS and DPS were the following: the average molecular weights were 115,200 and 10,200, the carboxyl contents were 13.8% and 11.8%, the intrinsic viscosities [η] were 0.498 and 0.1056 L/g, and the solubilities were 8 and 40 g/L, respectively. Conventional chemicals, such as potassium oxalate (K_2Oxa) and $CaCl_2$, were of analytical grade.

African green monkey renal epithelial cells (Vero) were purchased from Shanghai Cell Bank (China). The cell proliferation assay kit (Cell Couting Kit 8, CCK-8) was purchased from Dojindo Laboratory (Kumamoto, Japan). Superoxide dismutase kit (SOD) was purchased from the Jiancheng Institute of Biotechnology of Nanjing (China). Cell culture plates were purchased from Iwaki (Japan).

2.2. Apparatus

The XL-30 type environmental scanning electron microscope (ESEM) was from Holland Philips Company. The Optima 2000DV inductively coupled plasma atomic emission spectrometry (ICP-AES) was from America PE Co. The Fourier transform infrared spectrometer (FT-IR) was from America Nicolet Co. The D/Max 2400 type X-ray powder diffraction was from Rigaku, Japan. The Zatasizer 300HS nanoparticle size-Zeta potential analyzer was from Malvern, England. The Enzyme Mark Instrument was from Safire2, Tecan, Switzerland.

2.3. Crystallization of CaOxa

$CaCl_2$ solution (20 mL, 30 mmol/L) and different volumes of DPS or SPS were mixed in a beaker, diluted to 30 mL with double-distilled water, and then stirred with a magnetic stirrer for 10 min. Afterward, 30 mL of 20 mmol/L K_2Oxa solution was added. The final concentrations of $CaCl_2$ and K_2Oxa were both 10 mmol/L, and the concentrations of polysaccharide were from 0 g/L to 0.60 g/L. After 10 min of reaction, the suspension was centrifuged, and the concentration of soluble Ca^{2+} ions in the supernatant was measured using the ICP-AES method. CaOxa precipitates were dried for component analysis using XRD and FT-IR, and some precipitates were ultrasonically dispersed with anhydrous alcohol to observe the morphology by SEM.

The relative percentage contents of COM and COD in CaOxa precipitates were calculated by the *K* value method according to the XRD patterns (Donnet, Jongen, Lemaitre, & Owen, 2000).

2.4. Zeta potential measurement of CaOxa crystals

CaOxa crystals (10.0 mg), precipitated under different conditions as previously described, were dissolved in 30 mL double-distilled water and ultrasonically processed for 10 min. The Zeta potential of the suspension was measured using the Zeta potential analyzer.

2.5. Repair effect of DPS on the renal epithelial cells (Vero) of the African green monkey

The culture, injury, and repair of Vero cells were performed in an incubator at 37 °C with 5% CO_2 and saturated humidity as previously described (Ouyang et al., 2011). The cells were divided into three groups. For the control group, only serum-free medium was added. For the injury group, serum-free medium containing H_2O_2 (the final concentration was 0.3 mmol/L) was added to the cells for 1 h, and the cells were oxidatively injured. Then, the injured cells were rinsed twice with PBS and were prepared for the succeeding experiments. For the repair group, 1 and 10 μg/mL of DPS were added into the injured cells for 2 h. Then, the cell morphologies in the three groups were observed. Cell viability was then determined using the CCK-8 method, and the extracellular SOD activity was measured using the SOD kit.

The following procedures were performed to detect cell viability. After the cells were trypsinized, 100 μL of cell suspension (1×10^5 cells/mL) was plated in 96-well plates and cultured in DMEM/F12 containing 10% newborn calf serum for 24 h. The medium was then aspirated, and the cells were kept in the serum-free medium for 12 h to achieve quiescence. Afterward, the cells were divided into three groups: the control, injury, and repair groups. CCK-8 (10 μL) was added into each well. After 4 h of incubation, absorbance (A) was measured using the enzyme mark instrument at 450 nm. Three wells were measured in parallel under the same conditions to obtain the average value of *A*. Cell viability was calculated using $A_{exp}/A_{con} \times 100\%$, where A_{exp} is the absorbance of the cells exposed to the reagents and A_{con} is the absorbance of the control cells.

For the SOD activity measurement, the cell suspension with a concentration of 1×10^5 cells/mL was inoculated into 24-well plates (500 μL per well) and cultured in the incubator at 37 °C with 5% CO_2. After synchronization, the cells were divided into three groups: the control, injury, and repair groups. The experiment was repeated thrice. SOD activity in the supernatant was examined using the SOD kit.

To determine the regulation of cells on CaOxa crystal growth, the cell suspension was inoculated into 12-well plates with a final concentration of 1×10^5 cells/mL (1 mL per well) and with cover

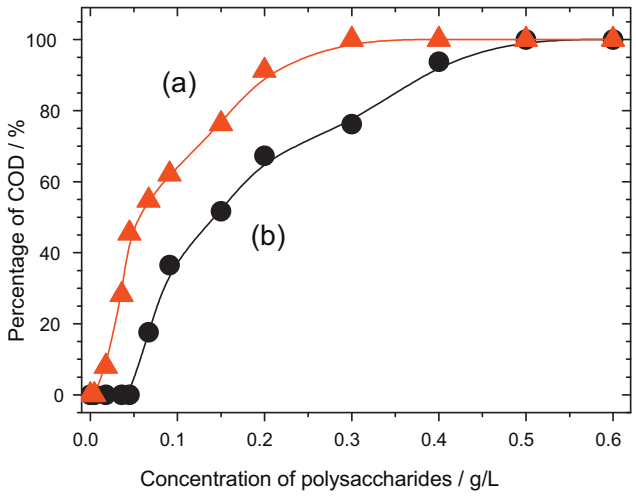

Fig. 1. Induction capacity comparison of the different concentrations of DPS and SPS on COD formation: (a) DPS and (b) SPS.

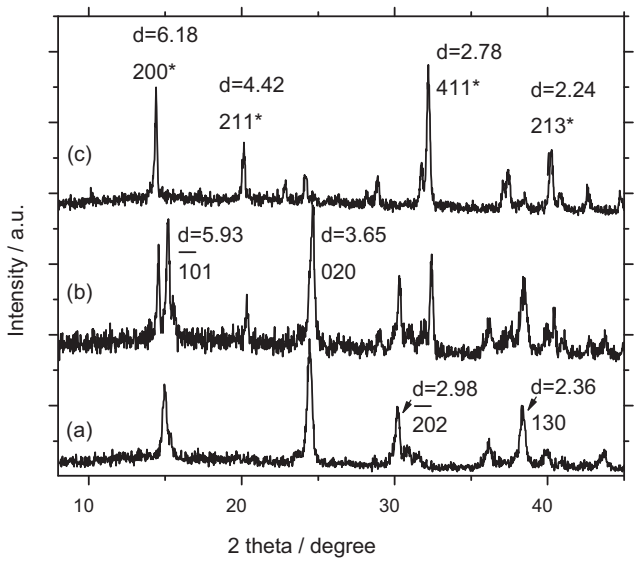

Fig. 2. XRD patterns of CaOxa precipitates formed in the presence of different concentrations of DPS: (a) 0.0045; (b) 0.045 and (c) 0.30 g/L. c(CaOxa) = 10.0 mmol/L. The crystal faces marked with an asterisk indicate COD and those without an asterisk refer to COM.

slips at the bottom. A large area of the cover slips was covered with cells after 24 h of incubation, and then the media were changed to serum-free DMEM-F12 for 12 h of synchronization. The cells were divided into three groups: the control, injury, and repair groups. A serum-free medium containing 0.5 mmol/L of CaOxa was added to each group. After 6 h of incubation, the cover slips were removed and washed with D-Hanks thrice, and then fixed with 2.5% glutaraldehyde for 24 h. The cells were washed again thrice with D-Hanks, dehydrated in gradient ethanol (30%, 50%, 70%, 90%, and 100%, subsequently), washed thrice with isoamylacetate, dried under the critical point of CO_2, and embedded via gold sputtering. The cell morphology and crystal growth in the three groups were observed through SEM.

3. Results and discussion

3.1. Inhibition of DPS on CaOxa growth, aggregation and induction on COD formation

3.1.1. XRD analysis

Fig. 1 shows the relative mass percentage of COD in CaOxa precipitates after adding different concentrations of DPS or SPS as quantitatively calculated using the K value method, according to the previously described XRD spectra (Donnet, Jongen, Lemaitre, & Owen, 2000). The following can be concluded:

(1) For both DPS and SPS, the relative mass percentage of induced COD crystals increased with enhanced c(DPS) or c(SPS).
(2) For DPS, when c(DPS) was less than or equal to 0.0045 g/L, only COM crystals formed, and the XRD patterns revealed diffraction peaks of COM crystals attributed to the planes of $(\bar{1}\,0\,1)$, $(0\,2\,0)$, $(\bar{2}\,0\,2)$, and $(1\,3\,0)$ (Fig. 2a). In contrast, c(DPS) increased to 0.30 g/L, diffraction peaks of COM disappeared completely, and the remaining products were all COD crystals (Fig. 2c), with the main diffraction peaks corresponding to the $(2\,0\,0)$, $(2\,1\,1)$, $(4\,1\,1)$, and $(2\,1\,3)$ planes.
(3) For the un-degraded SPS, COD crystals appeared only when c(SPS) increased to 0.067 g/L; 100% induction of COD crystal formation occurred at 0.50 g/L of SPS.

These results show that DPS exhibited a much stronger ability to induce and to stabilize COD crystals compared with SPS, which may be attributed to the following reasons:

(1) DPS is an anionic polymer and contains up to 11.8% of carboxylic acid group (COO^-)[8], whereas the $(\bar{1}\,0\,1)$ plane of COM crystals was positively charged (Qiu et al., 2005). Therefore, these polysaccharide molecules with negative charges (COO^-) could adhere to the COM surface through electrostatic interaction, which prevents the further deposition of Ca^{2+} ions on COM surface and inhibits the growth of COM. In contrast, the COD surface is electrically neutral (Jung, Kim, & Choi, 2004; Jung, Sheng, et al., 2004), which indicates the weaker adsorption ability to DPS. Therefore, DPS simultaneously promotes the growth of COD crystals and inhibits the formation of COM crystals.
(2) Abundant Ca^{2+} ions were regionally enriched at the surface of DPS after the acid group of DPS chelated with Ca^{2+} ions, resulting in the formation of a high-energy interface. In addition, the freedom degree of adsorbed Ca^{2+} ions decreased, whereas the energy state increased. The aforementioned high-energy interface and the Ca^{2+} ions at the high-energy state both facilitated the generation of thermodynamic metastable COD.
(3) The absorption of Ca^{2+} ions on the DPS surface led to a significant increase in Ca^{2+} ion concentration on the surface than in the bulk; hence, the positive/negative ion ratio (R_i,R_i = $[Ca^{2+}]/[Oxa^{2-}]$) diverged from the stoichiometric ratio of crystals. Excessive Ca^{2+} ions ($R_i > 1.0$) facilitate the formation of COD crystals, and excessive Oxa^{2-} ions ($R_i < 1.0$) facilitate the formation of COM crystals (Jung, Kim, et al., 2004). Thus, the adsorption of Ca^{2+} by DPS promoted COD formation.

COD had a smaller surface area than COM, thus, its contact intensity to renal tubular cells was lower than that of COM (Wesson, Worcester, Wiessner, & Mandel, 1998), i.e., COD crystals would be more easily excreted with urine than COM crystals. Therefore, inducing more COD formation in CaOxa crystals can prevent the formation of urinary stones. DPS may be a potential green drug for preventing the formation of urinary stones.

3.1.2. FT-IR analysis

The FT-IR spectra of CaOxa crystals in the presence of different DPS concentrations were determined. The representative spectra are shown in Fig. 3. Fig. 3a and b shows the CaOxa precipitates that are produced when the DPS concentrations were 0.0045 and

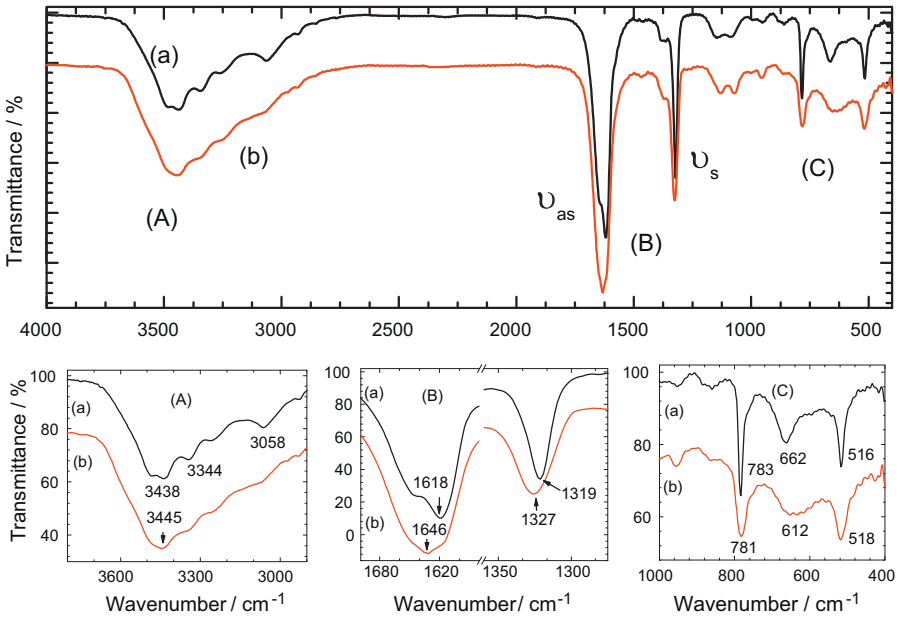

Fig. 3. FT-IR spectra of CaOxa precipitates formed in the presence of different concentrations of DPS: (a) 0.0045 and (b) 0.30 g/L. *c*(CaOxa) = 10 mmol/L.

0.30 g/L, respectively. All products were COM crystals in the former condition, which became COD crystals in the final condition. Fig. 3a and b illustrates the following distinct differences:

(1) The shape and intensity of crystal water absorption peaks were different (A area in Fig. 3). For COM crystals, the 3000 cm^{-1} to 3600 cm^{-1} region had multiple peaks, whereas COD crystals (Fig. 3b) only had a single absorption peak at 3445 cm^{-1}.
(2) In the B area of Fig. 3a, the asymmetrical stretching vibration $\upsilon_{as}(COO^-)$ of carbonyl appeared at 1618 cm^{-1}, whereas the $\upsilon_s(COO^-)$ appeared at 1319 cm^{-1}, both indicating the presence of COM crystals (Girija, Latha, Kalkura, & Subramanian, 1998; Ouyang, Duan, & Tieke, 2003). In Fig. 3b, the $\upsilon_{as}(COO^-)$ and $\upsilon_s(COO^-)$ occurred at approximately 1646 and 1327 cm^{-1}, respectively, indicating the presence of COD.
(3) In the fingerprint region (C area), the absorption peak at 783 cm^{-1} in Fig. 3a was very sharp and corresponded to COM, whereas the peak of COD at 783 cm^{-1} was weaker and wider. The appearance at 662 and 612 cm^{-1} could further indicate COM and COD crystals, respectively.

When the DPS concentration ranged from 0.0045 g/L to 0.30 g/L, varying blue-shifts of $\nu_{as}(COO^-)$ and $\nu_s(COO^-)$ appeared (Fig. 4), ranging from 1618 cm^{-1} to 1646 cm^{-1} (Fig. 4a) and from 1319 cm^{-1} to 1327 cm^{-1} (Fig. 4b), respectively. This showed that the precipitates were a mixture of COM and COD crystals, and the percentage of COD crystals in the precipitates gradually increased, which were consistent with the corresponding XRD results. Moreover, the curve in Fig. 4 rapidly increased, initially, and then increased at significantly slower rates; the slower increase may be attributed to the vibration strength of COM, which is two to three times higher than that of COD (Laurence, Levillain, Lacour, & Daudon, 2000). Thus, the blue-shifts of $\nu_{as}(COO^-)$ and $\nu_s(COO^-)$ were not proportional to the percentage of COD crystals in the COM–COD mixture.

3.1.3. SEM observation

Fig. 5 shows the crystal morphologies of DPS-induced COM and COD, wherein the following were observed:

(1) When the concentration of DPS was 0.0045 g/L, CaOxa existed as flake crystals with clear edges and corners, as well as significant aggregation (Fig. 5a). XRD (Fig. 2a) and FT-IR (Fig. 3a) revealed that these crystals were COM crystals.
(2) When DPS concentration increased to 0.045 g/L, CaOxa crystals showed blunt edges and weaker crystal aggregation (Fig. 5b), and these crystals were a mixture of COM–COD crystals (Fig. 2b). The fact that DPS can inhibit COM crystal aggregation can be attributed to the negative Zeta potential on the crystal surface after DPS adhered to positively charged COM crystals (Fig. 6), which produced an enhanced electrostatic repulsive force among the COM crystals.
(3) When DPS concentration further increased to 0.30 g/L, most CaOxa crystals became blunt (Fig. 5c), with a significantly increased dispersion degree and small aggregation, and the XRD results indicated that the crystals were COD (Fig. 2c). The following reasons may show why DPS induced the formation of COD microcrystallines with blunter edges and corners. The acid groups in DPS molecules can interact with Ca^{2+} ions on the COD crystal surface, particularly on the crystal edges, to reach

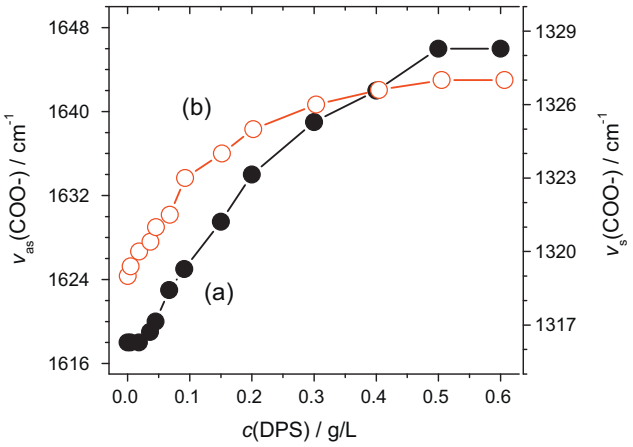

Fig. 4. Effect of DPS concentration on the wavenumber of the main peaks of CaOxa crystals: (a) $\nu_{as}(COO^-)$ and (b) $\nu_s(COO^-)$.

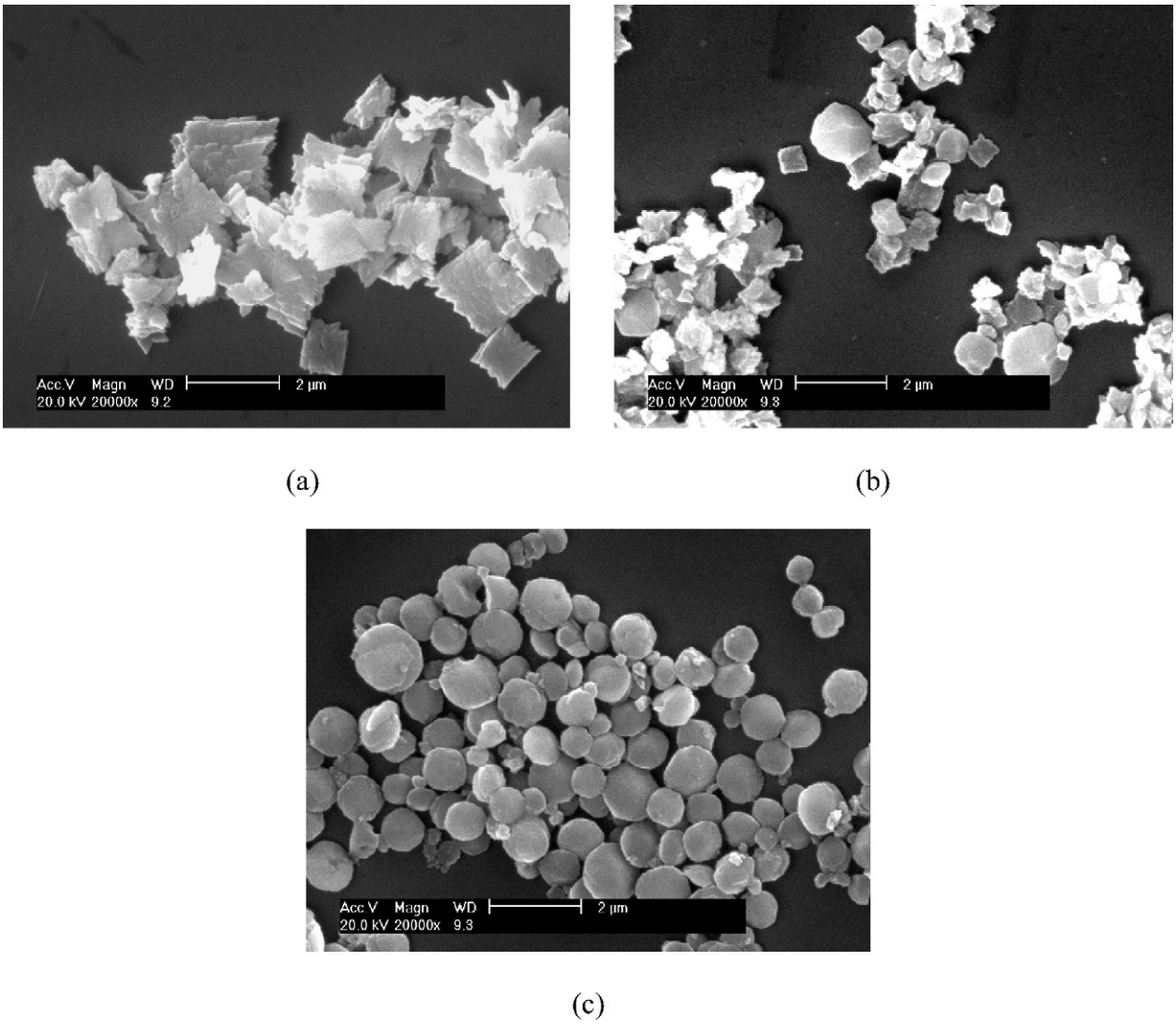

Fig. 5. SEM images of CaOxa precipitates formed in the presence of various concentrations of DPS: (a) 0.0045; (b) 0.045 and (c) 0.30 g/L. *c*(CaOxa) = 10 mmol/L.

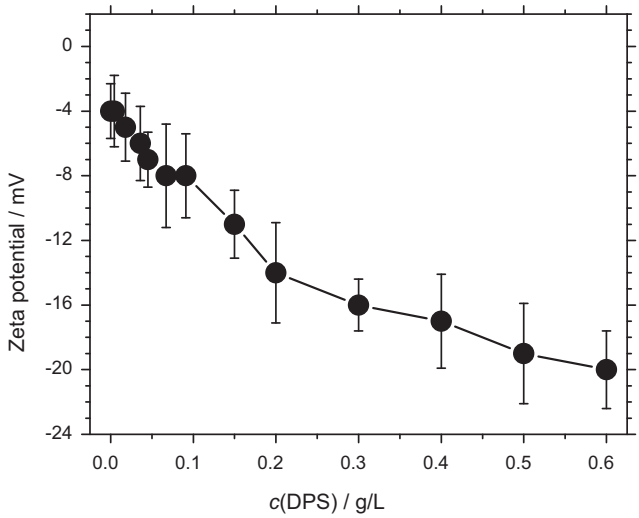

Fig. 6. Zeta potentials of CaOxa crystal suspension in the presence of different concentrations of DPS.

a dissolution–complexation balance, which leads to a constant dissolution-deposition of CaOxa crystals, and eventually, to the edges becoming blunt. These scattered COD crystals with blunt edges are more easily excreted due to their small surface area and weak adhesion to the urinary cell surface. Therefore, compared with the COD crystals with sharp edges, the blunt COD crystals are more conducive to the inhibition of the formation of CaOxa stones.

3.1.4. Zeta potential of CaOxa suspension

The Zeta potentials of CaOxa crystal suspension are shown in Fig. 6. As DPS concentration increased from 0 g/L to 0.60 g/L, the Zeta potentials of the induced CaOxa crystals reduced from −4 mV to −20 mV, which can be attributed to the positively charged surface of COM crystals (Qiu et al., 2005), whereas that of COD crystals were nearly neutral (Jung, Kim, et al., 2004; Jung, Sheng, et al., 2004). Thus, the Zeta potentials of the crystal surface were weaker before chelating with DPS, and then became negative after the crystal surface was covered with a layer of negatively charged polysaccharide molecules. The repulsive force among crystals increased after the Zeta potential became negative, which inhibited the crystal aggregation and deposition from urine.

Table 1
Concentration of soluble Ca^{2+} ions in the supernatant after the precipitation of calcium oxalate as determined by ICP-AES/μmol/L.

Conc./g/L	0	0.0045	0.045	0.067	0.10	0.15	0.30	0.50
DPS	49	52	88	102	141	185	267	301
SPS	49	52	79	97	130	168	229	276

3.1.5. Measurement of soluble Ca^{2+} ions by ICP-AES

The concentration of soluble Ca^{2+} ions in the supernatant was measured using ICP-AES after CaOxa precipitates were separated (Table 1). As DPS concentration increased, the soluble Ca^{2+} ions concentration also increased. At the same concentration, DPS could induce a higher concentration of soluble Ca^{2+} ions compared with SPS; however, the soluble Ca^{2+} concentrations at both conditions were higher than that of the blank control group (49 μmol/L).

The enhanced soluble Ca^{2+} concentration was due to the complexation between Ca^{2+} and SPS, particularly the degraded DPS. The concentration of soluble Ca^{2+} ions in the system was higher than that with the same concentrations of SPS because the molecular chain of DPS greatly shortened and its ability to chelate Ca^{2+} ions became stronger, i.e., compared with SPS, DPS showed a stronger inhibition on CaOxa crystallization and CaOxa precipitate formation.

3.2. Repair effect of DPS on injured Vero cells

3.2.1. Changes in the cell viability and extracellular SOD activity of Vero cells before and after DPS repair

The repair effect of DPS on injured Vero cells was investigated. Cell viability was 100 ± 6.6% in the control group, whereas it decreased to 72.1 ± 4.1% ($P < 0.05$) after being injured by 0.30 mmol/L of H_2O_2 for 1 h, indicating that Vero cells were seriously injured by H_2O_2.

After repairing with DPS, the cell viability of injured Vero increased and showed a positive correlation with DPS concentration. To illustrate, at 1 and 10 μg/mL DPS concentrations, the Vero viability was 80.2 ± 5.1% and 87.5 ± 6.1% ($P < 0.05$), respectively. Thus, DPS could effectively repair injured Vero cells in a dose-dependent manner.

After the repair by DPS, the extracellular SOD activity of Vero also increased, indicating the improved ability to scavenge free

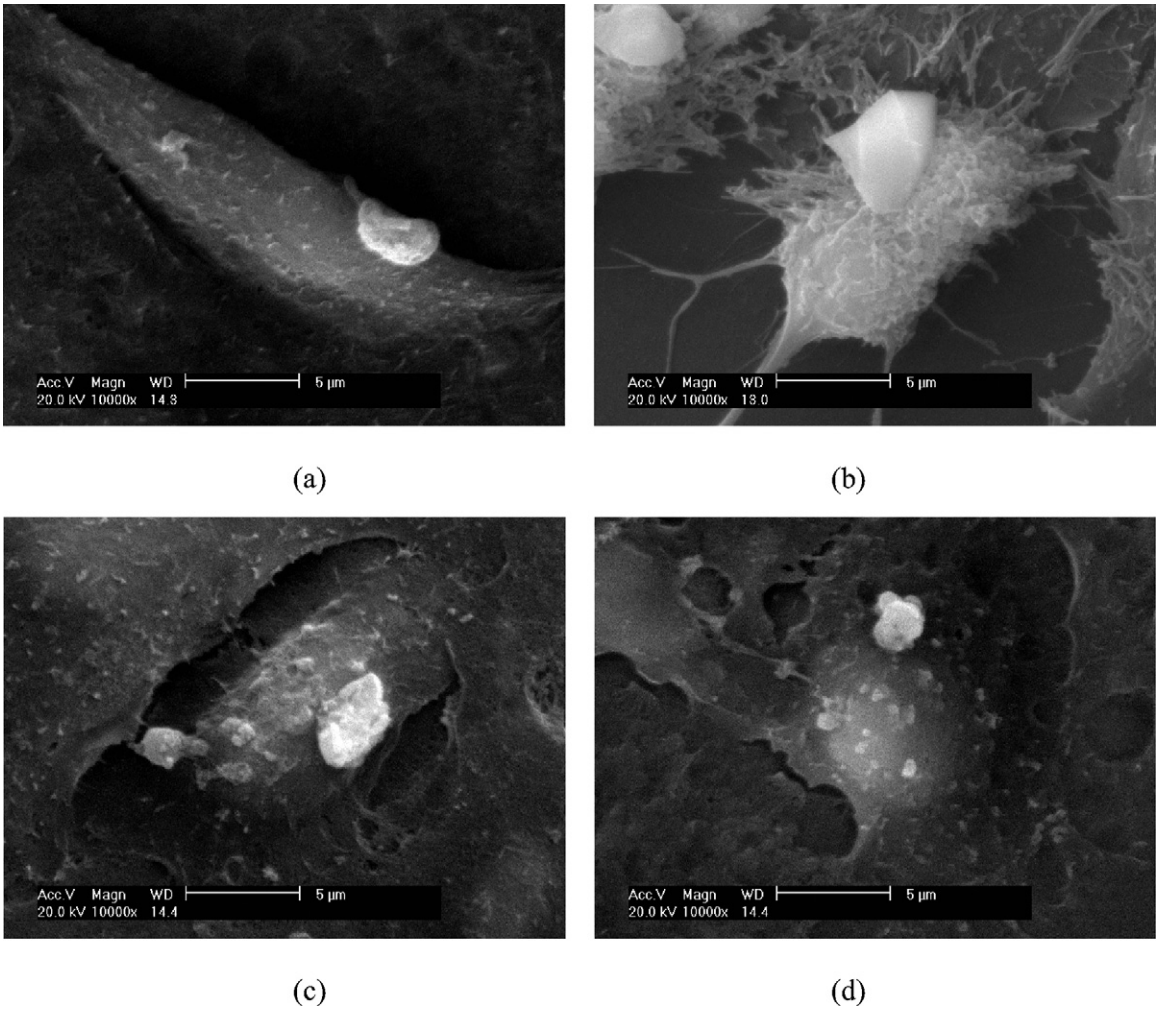

Fig. 7. SEM images of CaOxa crystals induced by different states of Vero: (a) control group; (b) injury group and (c) repair group I: c(DPS) = 1 μg/mL; (d) repair group II: c(DPS) = 10 μg/mL. Repair time: 2 h. Crystallization conditions: c(CaOxa) = 0.5 mmol/L; t = 6 h.

radicals. The SOD activity of Vero was 11.2 ± 0.3 U/mL in the control group, whereas it declined to 8.5 ± 0.4 U/mL ($P < 0.05$) after H_2O_2 injury. After the repair by 1 and 10 μg/mL DPS, the SOD activity increased to 9.9 ± 0.5 and 11.3 ± 0.6 U/mL ($P < 0.05$), respectively.

3.2.2. Differences of Vero cell induction on CaOxa crystals before and after repair

Fig. 7 shows the SEM images of CaOxa crystals induced by different states of Vero cells in 0.5 mmol/L of CaOxa solution. The following were observed:

(1) The CaOxa crystals induced by normal Vero were in lower quantity and in smaller size, indicating that the surface of normal Vero could inhibit the crystal growth.
(2) Compared with normal Vero, injured Vero-induced CaOxa crystals showed a significantly increased quantity as well as size with sharp edges (Fig. 7b). The injured cells expressed various negatively charged materials on their upper membrane surface (Fong-ngern, Peerapen, Sinchaikul, Chen, & Thongboonkerd, 2011; Ouyang, Yao, Tan, & Wang, 2011), such as hyaluronic acid, collagen protein, and osteopontin (OPN). After the negatively charged materials were distributed on the cell membrane surface, they became the sites that adsorb the Ca^{2+} ions and positively charged COM microcrystallines, thereby promoting the nucleation, growth, and adhesion of CaOxa crystals (Ouyang, Yang, & Tan, 2010). Thus, cell injury tends to enhance the risk of kidney stone formation.
(3) When the injured Vero cells were repaired by 1 and 10 μg/mL DPS for 2 h (Fig. 7c and d), the size of the induced CaOxa crystals gradually decreased, and the edges and corners of the crystals became blunter, which may be attributed to the capability of injured cells to resist crystal growth and gradual recovery after repair. Compared with the CaOxa crystals with irregular shape and sharp edges, the blunt crystals cannot easily adhere to the cell, thereby causing relatively lesser harm to the cells (Ouyang et al., 2011).

4. Conclusions

DPS can effectively increase the concentration of soluble Ca^{2+} in the system, inhibit the growth and aggregation of COM, induce the generation of COD, and blunt the edges of CaOxa crystals. DPS exhibited a much stronger ability to induce and stabilize COD crystals compared with SPS. DPS exhibited a distinct repair effect on H_2O_2-injured Vero cells in a dose-dependent manner. The repaired cell showed increased cell viability and extracellular SOD activity. The capability of the three states of Vero to inhibit CaOxa growth and adhesion follows this trend: control group > repair group > injury group. The repaired cells can reduce the formation of CaOxa crystals with sharp edges and corners, as well as decrease the size and quantity of crystals. Thus, repair of the injured renal epithelial cells can reduce the risk of kidney stone formation. The results indicated that DPS may be a potential green drug for the prevention and treatment of kidney stones.

Acknowledgments

This work was supported by the National Natural Science Foundation of China (20971057), and the Scientific Research Foundation for the Returned Overseas Chinese Scholars, State Education of China.

References

Donnet, M., Jongen, N., Lemaitre, J., & Owen, P. (2000). New morphology of calcium oxalate trihydrate precipitated in a segmented flow tubular reactor. *Journal of Materials Science Letters*, *19*, 749–750.
Fong-ngern, K., Peerapen, P., Sinchaikul, S., Chen, S. T., & Thongboonkerd, V. (2011). Large-scale identification of calcium oxalate monohydrate crystal-binding proteins on apical membrane of distal renal tubular epithelial cells. *Journal of Proteome Research*, *10*(10), 4463–4477.
Funami, T., Nakauma, M., Noda, S., Ishihara, S., Asai, I., Inouchi, N., et al. (2008). Effects of some anionic polysaccharide on the gelatinization and retrogradation behaviors of wheat starch: Soybean-soluble polysaccharide and gum arabic. *Food Hydrocolloids*, *22*(8), 1528–1540.
Girija, E. K., Latha, S. C., Kalkura, S. N., & Subramanian, C. (1998). Crystallization and microhardness of calcium oxalate monohydrate. *Materials Chemistry and Physics*, *52*, 253–257.
Holmer, E., Kurachi, K., & Sodertrom, G. (2002). The molecular-weight dependence of the rate-enhancing effect of heparin on the inhibition of thrombin by antithrombin. *Biochemistry*, *193*, 395–400.
Jung, T., Kim, W. S., & Choi, C. K. (2004). Biomineralization of calcium oxalate for controlling crystal structure and morphology. *Materials Science and Engineering: C Materials for Biological Applications*, *24*, 31–33.
Jung, T., Sheng, X. X., Choi, C. K., Kim, W. S., Wesson, J. A., & Ward, M. D. (2004). Probing crystallization of calcium oxalate monohydrate and the role of macromolecule additives with in situ atomic force microscopy. *Langmuir*, *20*, 8587–8596.
Laurence, M. E., Levillain, P., Lacour, B., & Daudon, M. (2000). Advantage of zero-crossing-point first-derivative spectrophotometry for the quantification of calcium oxalate crystalline phases by infrared spectrophotometry. *Clinica Chimica Acta*, *298*, 1–11.
Le, X. T., Yin, H. P., & Xu, S. J. (2006). Preparation of low molecular weight polysaccharide of *Spirulina Platensis* and anti-tumor activity of its sulfates ester in vitro. *Pharmaceutical Biotechnology*, *13*(2), 119–122.
Lee, H. J., Jeong, S. J., Lee, H. J., Lee, E. O., Bae, H., Lieske, J. C., et al. (2011). 1,2,3,4,6-Penta-O-galloyl-βeta-D-glucose reduces renal crystallization and oxidative stress in a hyperoxaluric rat model. *Kidney International*, *79*(5), 538–545.
Li, J., Matsumoto, S., Nakamura, A., Maeda, H., & Matsumura, Y. (2009). Characterization and functional properties of sub-fractions of soluble soybean polysaccharide. *Bioscience Biotechnology & Biochemistry*, *73*(12), 2568–2575.
Lu, P., Hou, S. H., & Ouyang, J. M. (2010). Modulation of soluble soybean polysaccharide on formation of urinary crystal calcium oxalate. *Chinese Journal of Inorganic Chemistry*, *26*(1), 17–24.
Matsuo, M. (2008). Increased expression of heparan sulfate proteoglycan on the cultured renal epithelial cells during oxalate exposure. *The Kurume Medical Journal*, *55*(1 and 2), 19–28.
Ouyang, J. M., Duan, L., & Tieke, B. (2003). Effects of carboxylic acids on the crystal growth of calcium oxalate nanoparticles in lecithin water liposome systems. *Langmuir*, *19*, 8980–8985.
Ouyang, J. M., Wang, M., Lu, P., & Tan, J. (2010). Degradation of sulfated polysaccharide extracted from algal *Laminaria japonica* and its modulation on crystallization of calcium oxalate. *Materials Science and Engineering: C Materials for Biological Applications*, *30*, 1022–1029.
Ouyang, J. M., Yang, R. E., & Tan, J. (2010). Effect of renal epithelial cell after injury on biomineralization of calcium oxalate. *Progress in Chemistry*, *22*(8), 1665–1671.
Ouyang, J. M., Yao, X. Q., Tan, J., & Wang, F. X. (2011). Renal epithelial cell injury and its promoting role in formation of calcium oxalate monohydrate. *Journal of Biological Inorganic Chemistry*, *16*(3), 405–416.
Qiu, S. R., Wierzbicki, A., Salter, E. A., Zepeda, S., Orme, C. A., Hoyer, J. R., et al. (2005). Modulation of calcium oxalate monohydrate crystallization by citrate through selective binding to atomic steps. *Journal of the American Chemical Society*, *127*(25), 9036–9044.
Wesson, A. J., Worcester, M. E., Wiessner, J. H., & Mandel, N. S. (1998). Control of calcium oxalate crystal structure and cell adherence by urinary macromolecules. *Kidney International*, *53*, 952–957.
Yang, H., Dou, Y., Zheng, X., Tan, Y., Cheng, J., Li, L., et al. (2011). Cysteinyl leukotrienes synthesis is involved in aristolochic acid I-induced apoptosis in renal proximal tubular epithelial cells. *Toxicology*, *287*(1-3), 38–45.
Yao, X. Q., Deng, S. P., & Ouyang, J. M. (2011). Promotion on nucleation and aggregation of calcium oxalate crystals by injury of HKC cell. *Chemical Journal of Chinese Universities*, *32*, 236–240.
Yao, X. Q., Peng, H., Tan, J., & Ouyang, J. M. (2012). Differences on mediation of calcium oxalate crystal growth by Vero cells before and after repaired. *Chinese Journal of Inorganic Chemistry*, *28*, 459–464.
Yao, X. Q., Tan, J., Lu, P., & Ouyang, J. M. (2011). Degradation of soybean polysaccharide and its inhibition on the growth of calcium oxalate. *Journal of Jinan University Natural Science & Medicine Edition*, *32*(1), 61–65.
Yasir, F., & Waqar, M. A. (2011). Effect of indigenous plant extracts on calcium oxalate crystallization having a role in urolithiasis. *Urological Research*, *39*(5), 345–350.
Yu, S. L., Gan, X. G., Huang, J. M., Cao, Y., Wang, Y. Q., Pan, S. H., et al. (2011). Oxalate impairs aminophospholipid translocase activity in renal epithelial cells via oxidative stress: implications for calcium oxalate urolithiasis. *Journal of Urology*, *186*(3), 1114–1120.
Zhang, S., Su, Z. X., Yao, X. Q., Peng, H., Deng, S. P., & Ouyang, J. M. (2012). Mediation of calcium oxalate crystal growth on human kidney epithelial cells with different degrees of injury. *Materials Science and Engineering: C*, *32*, 840–847.